


Simple 3D spheroid cell culture model for studies of prion infection

Zuzana Fremuntova¹ | Zdenka Backovska Hanusova¹ | Jakub Soukup¹ |
Tibor Mosko¹ | Radoslav Matej² | Karel Holada¹ 

¹Institute of Immunology and Microbiology, First Faculty of Medicine, Charles University, Prague, Czech Republic

²Department of Pathology and Molecular Medicine, Third Faculty of Medicine, Charles University and Thomayer University Hospital, Prague, Czech Republic

Correspondence

Karel Holada, Institute of Immunology and Microbiology, First Faculty of Medicine, Charles University, Studnickova 7, 128 00 Prague 2, Czech Republic.
Email: karel.holada@lf1.cuni.cz

Funding information

Ministry of Health of the Czech Republic, Grant/Award Number: NU23-04-00173; European Union - Next Generation EU, Grant/Award Number: Programme EXCELES, ID Project No. LX22NPO5107; Grant Agency of Charles University, Grant/Award Number: GAUK 530217

Edited by: WeiXiang Guo

Abstract

Mouse neuronal CAD 5 cell line effectively propagates various strains of prions. Previously, we have shown that it can also be differentiated into the cells morphologically resembling neurons. Here, we demonstrate that CAD 5 cells chronically infected with prions undergo differentiation under the same conditions. To make our model more realistic, we triggered the differentiation in the 3D culture created by gentle rocking of CAD 5 cell suspension. Spheroids formed within 1 week and were fully developed in less than 3 weeks of culture. The mature spheroids had a median size of ~300 µm and could be cultured for up to 12 weeks. Increased expression of differentiation markers GAP 43, tyrosine hydroxylase, β-III-tubulin and SNAP 25 supported the differentiated status of the spheroid cells. The majority of them were found in the G0/G1 phase of the cell cycle, which is typical for differentiated cells. Moreover, half of the PrP^C on the cell membrane was N-terminally truncated, similarly as in differentiated CAD 5 adherent cells. Finally, we demonstrated that spheroids could be created from prion-infected CAD 5 cells. The presence of prions was verified by immunohistochemistry, western blot and seed amplification assay. We also confirmed that the spheroids can be infected with the prions de novo. Our 3D culture model of differentiated CAD 5 cells is low cost, easy to produce and cultivable for weeks. We foresee its possible use in the testing of anti-prion compounds and future studies of prion formation dynamics.

KEYWORDS

cell differentiation, neuronal cells, prion infection, prion protein, PrP, spheroid culture

Abbreviations: CAD, catecholaminergic Cath.a cell line; CAD 5 PrP^{-/-}, CAD 5 cells with ablated expression of PrP; CAD 5 RML, CAD 5 cells chronically infected with RML prions; GAP 43, growth associated protein 43; GFAP, glial fibrillary acidic protein; rPrP, recombinant prion protein; PrP^C, cellular prion protein; PrP^{TSE}, pathological isoform of prion protein; PI, propidium iodide; PK, proteinase K; RML, Rocky Mountain Laboratory prion strain; RT-QuIC, real-time quacking-induced conversion assay; SNAP 25, synaptosomal-associated protein 25; TH, tyrosine hydroxylase.

This is an open access article under the terms of the [Creative Commons Attribution](https://creativecommons.org/licenses/by/4.0/) License, which permits use, distribution and reproduction in any medium, provided the original work is properly cited.

© 2024 The Author(s). *European Journal of Neuroscience* published by Federation of European Neuroscience Societies and John Wiley & Sons Ltd.

1 | INTRODUCTION

Prion diseases are transmissible neurodegenerative disorders affecting animals as well as humans with no existing effective treatment (Colby & Prusiner, 2011). The infection is caused by the spreading of a conformational change in the cellular prion protein (PrP^C), thus forming its pathological variant (PrP^{TSE}). Whereas PrP^C is formed mostly by α -helices, PrP^{TSE} contains mainly β -sheets (Caughy et al., 2022). This causes PrP^{TSE} to be partially proteolytically resistant. During the disease, PrP^{TSE} is accumulated mainly within the brain of the infected individual (Prusiner, 1998). The mechanism of how PrP^{TSE} causes the disease remains unspecified (Hughes & Halliday, 2017), and we even do not understand the physiologic function of PrP^C, although many ideas have been suggested and tested (Martellucci et al., 2020; Watts et al., 2018). Prion diseases are studied in animal models (rodents, primates) as well as in vitro (Brandner & Jaunmuktane, 2017). Both approaches have their limitations. Cell cultures are cheaper, but the cultivation of continually dividing cells in monolayer on plastic surface does not represent the reality seen in the organisms and is thus far less relevant. The number of cell lines infectible with prions is limited, and some prion strains are difficult to propagate in vitro (Grassmann et al., 2013). Animal models correctly recapitulate the disease pathogenesis but are not considered to be ethical, the disease development takes a long time and the cost is high. Recently, 3D cell cultures have emerged as an interesting alternative. Based on the origin of the cells forming 3D culture, so-called spheres from primary stem cells and spheroids from the cells of immortalized cell lines can be produced. Neurospheres formed by neural stem cells derived from mouse embryo brain are capable of self-renewal and differentiation into three basic lineages: neurons, astrocytes and oligodendrocytes (Collins & Haigh, 2017; Reynolds & Weiss, 1992). The neurospheres have been used to examine the prion infection, although the number of studies is limited. The neurospheres kept in proliferative conditions were not able to propagate prions, but the neurospheres stimulated to form neurons and astrocytes could be infected (Herva et al., 2010). The infection of differentiated mouse neurospheres led to cytopathic changes and apoptosis (Giri et al., 2006; Iwamaru et al., 2013). Brain aggregates formed by the cells of dissociated mouse embryo brain are another type of 3D cell culture. Infection of brain aggregates with Rocky Mountain Laboratory (RML) prions led to degeneration of neuronal dendrites (Ahn et al., 2016). A complex 3D cultivation and

differentiation of human pluripotent stem cells lead to the production of cerebral organoids with developed domains resembling different brain regions (Lancaster et al., 2013). Recently, human cerebral organoids have been successfully infected with different types of human prions and represent new exciting model for studies of both, sporadic and genetic prion diseases (Walters & Haigh, 2023). Here, we present an inexpensive and simple method of 3D cell culture utilizing a mouse CAD 5 cell line. CAD 5 cells are often used as a prion infection model because they are able to propagate a number of murine prion strains (Mahal et al., 2007). In addition, CAD 5 cells are able to differentiate into cells morphologically resembling neurons upon serum withdrawal (Fremuntova et al., 2020). Spheroids can be formed from CAD 5 cells chronically infected with RML prions, or they can be infected with prions de novo, making this model interesting for prion research.

2 | MATERIALS AND METHODS

2.1 | Cells

CAD 5 cells are of neuron origin, derived from catecholaminergic Cath.a cell line (Mahal et al., 2007; Qi et al., 1997), and were provided by Charles Weissmann (The Scripps Research Institute, Jupiter, FL, USA). The cells were kept in Opti-MEM (Thermo Fisher Scientific) with 10% BGS (HyClone Bovine Growth Serum, GE Healthcare Life Sciences) and 100-U penicillin/streptomycin ml⁻¹ and passaged every 3–4 days. Before passage, the cells were washed with .5-mM EDTA in phosphate buffered saline (PBS) pH 7.4 to weaken the attachment to the surface. For experiments with infectious PrP^{TSE}, we used CAD 5 cells chronically infected with the RML prion strain (Janouskova et al., 2012). We also used CAD 5 PrP^{-/-} cells with no PrP^C expression prepared with CRISPR/Cas 9 technology (Fremuntova et al., 2020).

2.2 | Induction of CAD 5 differentiation

Differentiation of CAD 5 cells was induced, as we have shown earlier (Fremuntova et al., 2020). The cells were stimulated to start differentiation by removing sera and changing media. Approximately 10⁶ cells per 25 cm² flask were resuspended in DMEM/F12 (Thermo Fisher Scientific) with penicillin/streptomycin instead of Opti-MEM with serum. Media was changed every 2–3 days, resulting in differentiated cells within 5–7 days.

2.3 | Formation of spheroids

In order to get 3D cell culture, the cells were prevented from adhesion to the bottom of the tissue culture plastic using flasks with a non-treated bottom designated for suspension cultures (SPL Life Sciences, cat. n. 70325); 200,000 cells were seeded in Opti-MEM media with serum in a 25 cm² culture flask and have been under constant rocking since then using the MR-1 Mini-Rocker Shaker (Biosan, fixed tilt angle 7°, 25 oscillations per minute). Half of the media was changed for DMEM/F12 without serum after 72 h. Since then, 2/3 of the media was removed 2 times per week, and the same amount of DMEM/F12 was added, thus diluting the concentration of sera to a minimum to promote differentiation of the cells. Spheroids were taken into the experiments 3 weeks after seeding the cells if not stated otherwise.

2.4 | Infection of spheroids with prions

The RML prion strain was provided by Adriano Aguzzi (Institute of Neuropathology, University of Zurich, Switzerland) and further propagated in CD1 mice in the author's facility. Frozen brain samples collected from terminally ill or control CD1 mice were homogenized in PBS supplemented with 2-mM EDTA and 1-mM PMSF using glass beads and Mini BeadBeater (Biospec). Resulting 10% (w/v) brain homogenates were aliquoted and stored at -80°C. Prior to its usage, the brain homogenate was passed through a 29-gauge needle, diluted to 1% (w/v) with PBS and further mixed with the cell culture media to prepare .1% (w/v) solution. The mixture was then used to replace half of the media in flasks with spheroids to make the final concentration of inoculum .05% (w/v). Subsequently, the medium was changed after 3 days and then twice a week as described above. Unless stated otherwise, 1-week-old spheroids were subjected to the infection.

2.5 | Light microscopy of spheroids

The formation of spheroids derived from CAD 5 cells was monitored by light microscopy. Spheroids were cultured for 4 weeks as described above, and representative images were taken regularly. The Olympus IX70 inverted microscope, equipped with a ProgRes MFcool camera (Jenoptik) and operated by NIS-Elements AR software (Nikon Instruments), was used for this purpose; the total magnification was set at 40 times. Images were processed and supplemented with a scale bar using Fiji ImageJ software.

2.6 | Analysis of spheroid size

Images of spheroids were taken on Days 3, 5, 7, 10, 14, 18, 21 and 28. Each day, two pictures of spheroid culture were taken with 10–30 spheroids per image, depending on the age of the culture. The diameter of the spheroid was measured manually in the middle of the spheroid, and all spheroids were measured at the same angle (0°). Data were analysed in Fiji ImageJ software.

2.7 | Fluorescence microscopy

Spheroids were washed twice in 1 ml of PBS. Next, 100 µl of PBS containing 10-µM CellTrace Far Red dye (Invitrogen, cat. N. C34564) was added to the spheroids. Spheroids were incubated for 20 min in the dark and then 3 times washed with PBS. Samples were mounted in a chamber created from glass slides and imaged with Leica TCS-SP5 laser scanning confocal microscope or Olympus IX83 wide-field microscope equipped with silicon oil immersion objective (magnification 60 times). Data from TCS-SP5 were processed using Fiji ImageJ software, and data from IX38 were processed using cellSence Dimensions software (Olympus) with 3D constraint iterative deconvolution. Twenty spheroids have been analysed.

2.8 | Optical projection tomography (OPT)

To prepare samples, we used the clear, unobstructed brain imaging cocktails and computational analysis (CUBIC) method to make tissue transparent. Spheroids were fixed with 4% paraformaldehyde in PBS and washed twice in PBS for 5 min. Spheroids were then cleared with CUBIC-1 solution (Susaki et al., 2014) for 1, 3 or 8 days, followed by a solution change just before taking pictures. Images were taken using an 810-nm laser (Thorlabs, M810L3) and processed for background and rotation corrections in Fiji ImageJ software. For 3D reconstruction, NRecon (Bruker) software was used with a filtered back-projection algorithm. Seven spheroids have been analysed.

2.9 | Protein extraction and immunoblotting

Fresh cells or cell pellets kept at -80°C were lysed in buffer containing .5% Triton X-100, .5% sodium deoxycholate (w/v), 50-mM Tris-HCl pH 7.5 and 150-mM NaCl in the presence of protease inhibitors cComplete (Roche

Diagnostics, Basel, Switzerland) for 30 min on ice. The samples were mixed every 10 min. After that, samples placed on the ice were sonicated twice for 10 s at 35% intensity using Dynatech Sonic Dismembrator Model 300 (ARTEK) to support the cell disruption. To cleave the DNA, benzonase (.1 U μl^{-1} , Millipore) was added to samples. Next, the protein concentration was measured with a Pierce BCA protein assay kit (Thermo Fisher Scientific). To detect the infectious PrP^{TSE}, the sample was treated with 50 $\mu\text{g ml}^{-1}$ proteinase K (PK) for 30 min at 37°C while gently shaking (400 rpm). The protein cleavage was stopped with a 2-mM PMSF inhibitor (10 min, RT). PrP^{TSE} is resistant to PK cleavage and shows typical bands, whereas PrP^C is cleaved completely. To enhance the PrP^{TSE} detection level, some samples were subjected to precipitation of PrP by sodium phosphotungstate (NaPTA) (Levine et al., 2015). After the lysis of cells in PBS containing 2% sarkosyl (w/v) and benzonase (.1 U μl^{-1}) for 30 min at 37°C with gentle shaking, protein concentration was determined using BCA assay. PrP in samples was then precipitated by incubation of the lysate with .32% NaPTA supplemented with 2.72-mM MgCl₂ for 1 h at 37°C while gently shaking and subsequently centrifuged at 14,000 × RPM for 30 min at RT (Jouan B4i, fixed rotor) to obtain a PrP-rich pellet. All samples were prepared for electrophoresis by boiling for 5 min at 95°C in Laemmli buffer. Electrophoresis and western blotting were performed as described previously (Panigaj et al., 2011).

Following primary antibodies were used: anti-PrP 6D11 (mAb, IgG2a, cat. n. 808002, BioLegend, 2 $\mu\text{g ml}^{-1}$, recognizes epitope 93–109 in PrP^C [Uchiyama et al., 2017]), anti-PrP AH6 (mAb, IgG2a, TSE Resource Centre, .5 $\mu\text{g ml}^{-1}$ [Kostelanska & Holada, 2022]), anti-PrP D18 (supernatant, clone D18, dilution 1:10 recognizes the central part of PrP^C; CHO cells producing D18 antibody donated by Dennis Burton, The Scripps Research Institute, California, USA [Williamson et al., 1998]), anti- β -III-tubulin (monoclonal, clone 2G10, IgG2a, cat. n. T8578, Sigma-Aldrich, lot 011M4756, .1 $\mu\text{g ml}^{-1}$ [Oz et al., 2012]), anti-doublecortin (polyclonal, cat. n. D9693, Sigma-Aldrich, lot 087K4831, .1 $\mu\text{g ml}^{-1}$ [González-González et al., 2017]), anti-GAP 43 (monoclonal, clone 7B10, IgG2a, cat. n. G9264, Sigma-Aldrich, lot 039K4851, 7 $\mu\text{g ml}^{-1}$ [He et al., 2015]), anti-GFAP (polyclonal, IgG, cat. n. GTX108711, Genetex, lot 39981, .4 $\mu\text{g ml}^{-1}$ [Lee et al., 2019]), anti-tyrosine hydroxylase (monoclonal, clone LNC1, IgG1 κ , cat. n. MAB318, Millipore, lot 3202369, dilution 1:1000 [Zhang et al., 2016]), anti-SNAP 25 (polyclonal, IgG, cat. n. S9684, Sigma-Aldrich, lot 127K4796, 1.25–2.5 $\mu\text{g ml}^{-1}$ [Ye et al., 2017]). Following fluorescent secondary antibodies were used: goat anti-mouse AzureSpectra

700 conjugate (cat. n. AC2129, Azure Biosystems, .25 $\mu\text{g ml}^{-1}$), goat anti-rabbit AzureSpectra 800 conjugate (cat. n. AC2134, Azure Biosystems, .25 $\mu\text{g ml}^{-1}$), goat anti-human IgG H + L Alexa Fluor[®] 633 conjugate (polyclonal, cat. n. A-21091, Invitrogen, 4 $\mu\text{g ml}^{-1}$). The fluorescent signal was detected using Azure c600 Imaging System (Azure Biosystems). Ponceau staining was used as a control of protein loading. The density of bands on blots was quantified using Fiji ImageJ or AzureSpot software (Azure Biosystems).

2.10 | Flow cytometry

Media from the spheroids was removed, and 3 ml of PBS/5-mM EDTA was added. Spheroids were kept for 10 min on ice, followed by 10 min at 37°C. After this procedure, the cells weakened the attachment to each other and were resuspended in PBS/.5% BSA, resulting in single-cell suspension in concentration 2×10^3 cells μl^{-1} . Since then, the suspension has been kept on ice. Samples containing 10^5 cells in 50 μl of PBS/.5% BSA were incubated for 30 min in the dark on ice with phycoerythrin-conjugated primary antibodies (custom procedure, Exbio) against different epitopes of prion protein molecule—DC2 (recognizing N-terminal part, monoclonal, IgG2a, donated by Vladka Curin Serbec, Blood Transfusion Centre of Slovenia, Slovenia, final concentration 5 $\mu\text{g ml}^{-1}$ [Didonna et al., 2015]), AH6 (recognizing C-terminal part, monoclonal, IgG2a, TSE Resource Centre, Roslin Institute, UK, final concentration 35 $\mu\text{g ml}^{-1}$ [Glier & Holada, 2012]) and with isotypic control. Antibodies were previously titrated for their saturating concentrations. The staining was stopped by adding 1 ml of PBS and mixing, and then the cells were centrifuged (500 g, 3 min, 4°C) and resuspended in 300 μl of PBS/.5% BSA. The flow cytometer FACS Canto II (BD Biosciences) was calibrated daily before measurement using Cytometer Setup & Tracking Beads Kit (BD Biosciences). The dead cells were excluded from the analysis by propidium iodide staining (.1 $\mu\text{g ml}^{-1}$). The data were analysed and corrected with fluorescence spectral overlap compensation using the FlowJo software.

2.11 | Cell cycle analysis

The cells were washed with PBS/5-mM EDTA, and 10^6 cells were resuspended in 1 ml of cold PBS. The cell suspension was slowly added into 70% ethanol while mixing. The cells were fixed for 24 h at 4°C. Next, the cells were centrifuged (200 g, 10 min, 4°C), washed with cold PBS, and the cell nuclei were stained with 500 μl of propidium

iodide staining solution (PBS/.1% Triton X-100, 20 $\mu\text{g ml}^{-1}$ propidium iodide, 10- μl RNase A [CellCycle-FlowEx Kit, Exbio]) in RT in the dark for 30 min. The distribution into the cell cycle phases was determined using flow cytometry and the detection of DNA by propidium iodide (Pozarowski & Darzynkiewicz, 2004). Cell doublets were excluded by analysis of the fluorescent signal peak area and width on the scattergram. The cell cycle analysis was done with the Flow Jo software using the Dean-Jett-Fox model.

2.12 | Immunohistochemical staining of spheroids

To visualize the prion infection among the spheroid cells, spheroids were fixed by 3.8% formaldehyde in PBS and embedded in paraffin; 5- μm -thick sections of formalin-fixed and paraffin-embedded samples were deparaffinized, pretreated in 96% formic acid and 4M guanidine thiocyanate, and then incubated with two primary anti-prion protein antibodies, clone 6H4 (Prionics, Switzerland, dilution 1:3000 [Matej et al., 2012]) and clone 12F10 (Cayman Chemical, USA, dilution 1:8000 [Jankovska et al., 2022]) overnight at 4°C. A second layer for light microscopy visualization, consisting of secondary horseradish peroxidase-conjugated antibody (En Vision FLEX/HRP, Dako, Denmark), was applied for 20 min at room temperature. The samples were then incubated with DAB (Substrate Chromogen Solution, Dako, Denmark) for 10 min to visualize the reaction. Mayer's Hematoxylin Solution was used as a counterstain. Images were taken by light microscope Olympus BX53 at original magnification 200 \times and 400 \times . For staining with haematoxylin-eosin only, the samples were deparaffinized, rehydrated and stained according to standard haematoxylin-eosin protocol.

2.13 | Real-time quaking-induced conversion (RT-QuIC) assay

The detection of prion seeding activity in the cell homogenate samples (1 g protein/L in PBS) was done by second-generation RT-QuIC assay as described previously (Moško et al., 2021). The samples were serially diluted 10^{-1} – 10^{-8} in PBS buffer containing N-2 supplement (Gibco, Thermo Fisher, Prague, Czech Republic) and .1% SDS. All dilutions were analysed in quadruplicate; 2 μl of the diluted sample was added to 98 μl of the reaction mix. The reaction mix consisted of 10-mM phosphate buffer, pH 7.4; 300-mM NaCl; 10- μM thioflavin T; 1-mM EDTA; .002% SDS; and .1 mg ml^{-1} of recombinant shortened hamster

PrP (rHaPrP90–231). The assay was carried out in FLUOstar Omega plate reader (BMG LABTECH GmbH, Ortenberg, Germany) by alternating shaking (60 s, 700 rpm, double orbital) and rest (60 s) cycles at 55°C for 48 h. The fluorescence was measured every 15 min.

3 | RESULTS

3.1 | CAD 5 cells infected with prions are capable of differentiation in 2D culture

The CAD 5 cells chronically infected with RML prions (CAD 5 RML) were able to initiate cell differentiation after the change of media and serum withdrawal, similarly as we have shown in the non-infected cells previously (Fremuntova et al., 2020). Upon serum withdrawal, the majority of the cells stopped proliferating, and their morphology changed from round, spread cells to cells with neurites (Figure S1). However, in comparison with the non-infected cells, the CAD 5 RML cells remained longer in a proliferative state, and their differentiation process was slower (see Data S1). Similarly, PrP knock-out cells (CAD 5 PrP^{-/-}) lacking PrP^C displayed higher proliferating capacity in 2D culture compared with CAD 5 PrP^{+/+} cells (Figure S2).

3.2 | CAD 5 cells can proliferate in 3D and form spheroids

CAD 5 cells kept in flasks with non-adhesive surface and incubated on a rocking platform spontaneously formed 3D spheroids. Already on the third day after the seeding, there were loose cell aggregates with a median diameter of 151 μm (Figure 1a,b). During the time, the spheroids grew reaching a median size approx. 320 μm the 18th day. Since then, the size has remained stable. According to the light microscopy observations, spheroids were compactly formed from Day 7 (Figure 1a).

We were able to keep spheroids in culture for 12 weeks with no noticeable morphological change (data not shown). Cultivation beyond 12 weeks has led to higher cell mortality, resulting in gradual spheroid disintegration. During the spheroid culture, some cells were always found dead floating in the media (Figure 1a, little dots), and they were removed by its change. On the basis of OPT, we can say the spheroids are fully formed by cells; there is no cavity without the cells inside the CUBIC-cleared spheroids (Figure 2a). Proteins were non-specifically stained with CellTrace Far Red (Invitrogen); the dye diffuses through the cytoplasmic membrane and is cleaved by intracellular esterases creating fluorescence

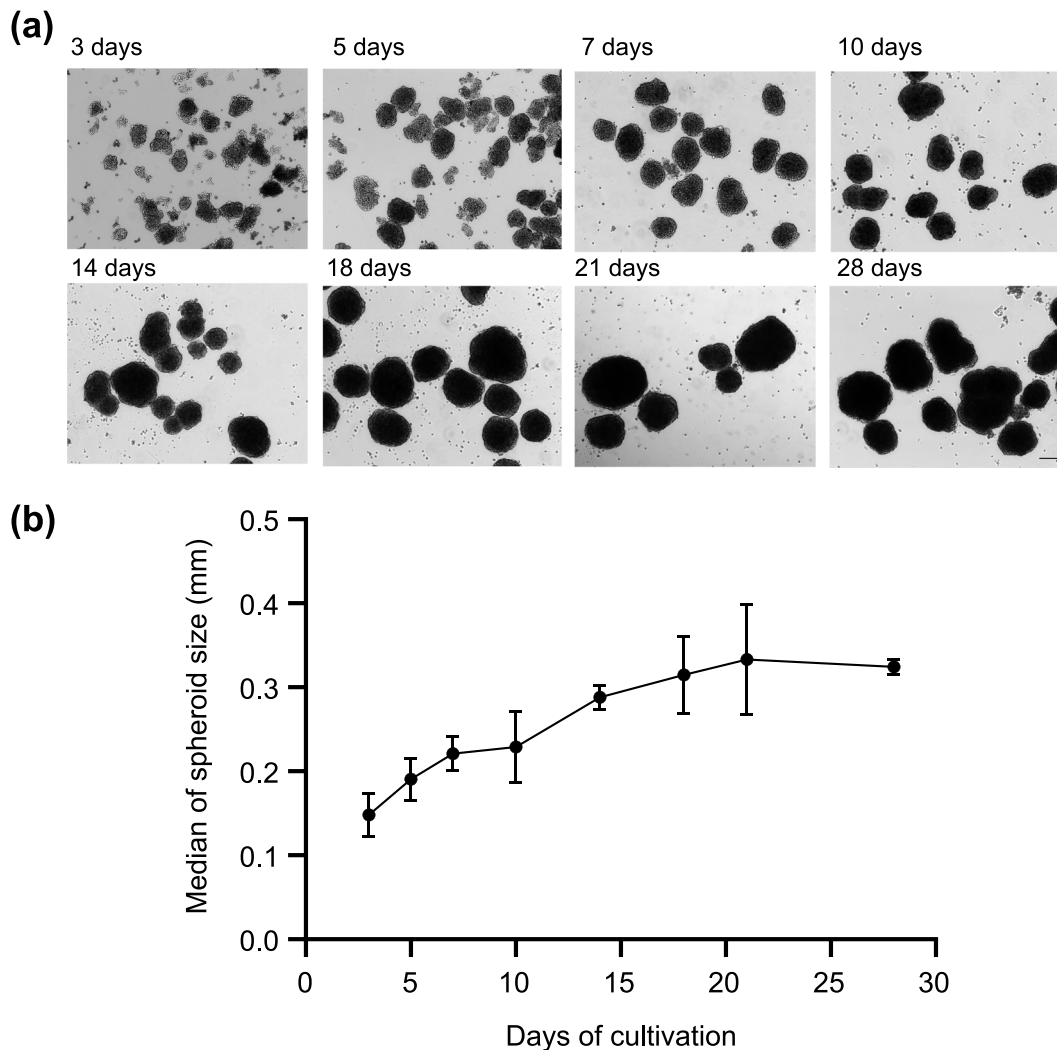


FIGURE 1 CAD 5 spheroids are compact cell aggregates cultivable for weeks. (a) Representative light microscopy pictures of spheroids' formation during the time. Scale bar: 250 μ m. (b) Quantitative analysis of spheroid size at different time points during their formation. Median \pm SD, $n = 3$ (Days 5, 10, 14, 18, 21), $n = 2$ (Days 3 and 28); in total, around 700 spheroids were measured.

compound that binds to free amines of proteins (Figure 2b). A video showing rotation of OPT and all planes of back-projection is provided in Supporting Information (Video S1 and S2).

3.3 | CAD 5 cells in spheroids show features of differentiated cells

To monitor the level of cell differentiation, we followed the expression of several neuronal differentiation markers using western blot (Figure S3). Densitometry analysis has suggested that CAD 5 cells in spheroids expressed 2 times more growth associated protein 43 (GAP 43), 1.7 times more tyrosine hydroxylase (TH), 1.2 times more β -III-tubulin and 1.4 times more synaptosomal-associated protein 25 (SNAP 25) than proliferating cells in monolayer (Figure 3a). On the other hand, the cells in spheroids

expressed only 18% of glial fibrillary acidic protein (GFAP) found in the proliferating cells in monolayer. There was no significant difference in the expression of doublecortin. Cells in the spheroids expressed 2.9 times more total PrP^C than the proliferating cells in the monolayer when detected with D18 antibody (Figure 3a).

3.4 | The surface expression of cell membrane PrP^C is similar in proliferating and spheroid CAD 5 cells, but there is more of a truncated form on the cell membrane of spheroid cells

Flow cytometry showed that there was no significant difference in the expression of PrP^C on the cell membrane of proliferating cells and cells in the spheroids (measured with AH6 antibody recognizing both full-length and

FIGURE 2 Spheroids are fully formed by cells. (a) Optical projection tomography: one of the original images of the cleared spheroid (left image) used for back-projection reconstruction (right images) of the spheroid. Plane images from back-projection reconstruction show that the spheroid is full of cells. Scale bar: 100 μm . (b) Confocal image of the cell trace far red labelled spheroids. The picture of the spheroid section shows intensive labelling of surface cells and limited labelling of spheroid inner cells. Scale bar: 50 μm .

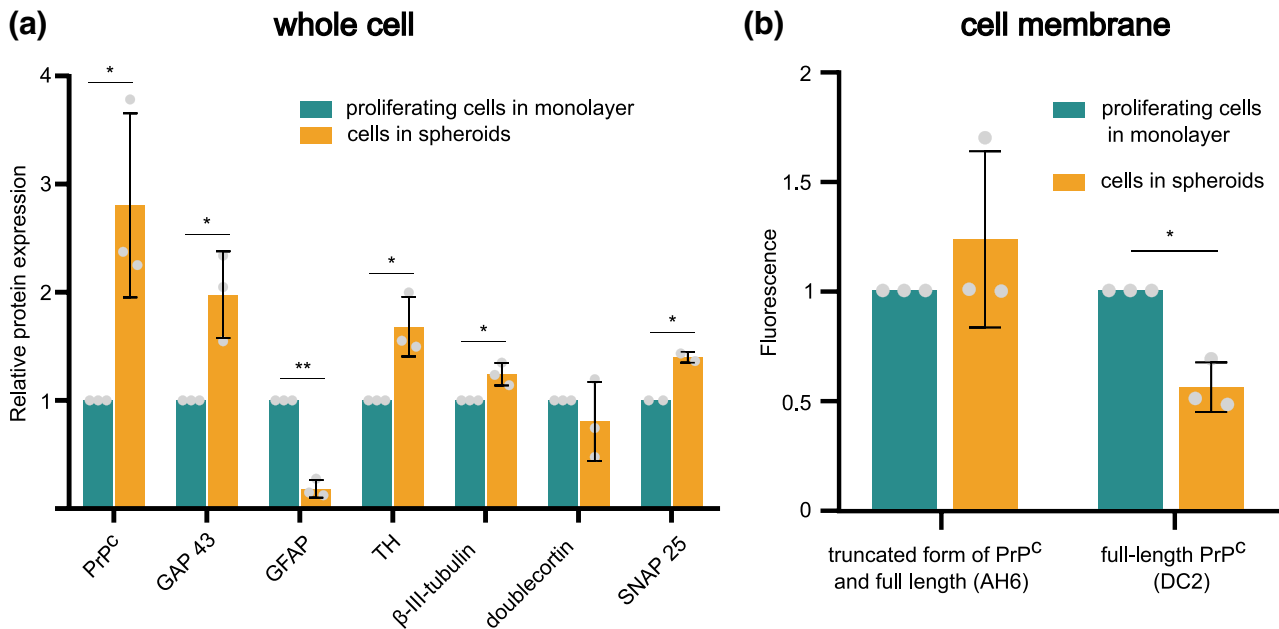
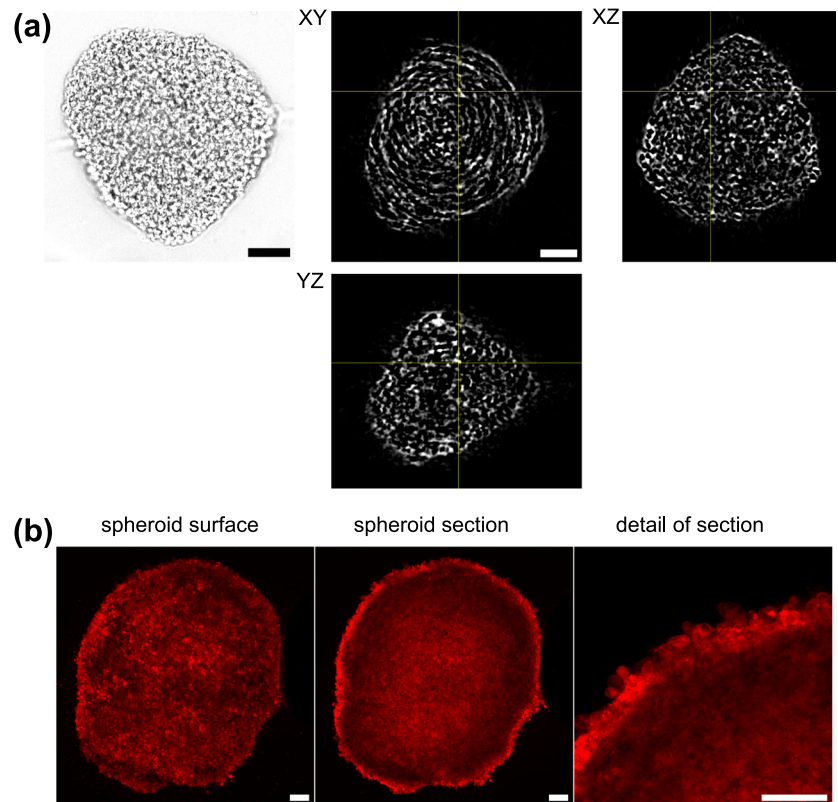


FIGURE 3 The relative expression of differentiation markers in 3D cultivated cells is different than in proliferating cells in 2D monolayer. (a) Densitometric analysis of differentiation markers by western blots. The density of protein bands in proliferating cells was assigned value 1, and the corresponding value of bands in spheroids was calculated. Mean \pm SD, $n = 3$ (n [SNAP 25] = 2). (b) Flow cytometric analysis of cell membrane expression of PrP^C. Antibody against C-terminus AH6 shows expression of both truncated and full-length PrP^C; N-terminal antibody DC2 detects only full-length PrP^C. Mean \pm SD, $n = 3$. Parametric or non-parametric t test, * $p < .05$, ** $p < .01$.

cleaved PrP^C) (Figure 3b). On the other hand, there was only 56% of full-length PrP^C on the cell membrane of spheroid cells compared with the cell membrane of proliferating CAD 5 cells (measured with DC2 antibody recognizing full-length PrP^C only).

3.5 | The majority of CAD 5 cells in spheroids stopped dividing

Cell cycle analysis showed that the majority of the spheroid cells were found in the G0/G1 phase (84.4%), and only 7.9% and 5% were found in the S and G2/M phases

of the cell cycle, respectively (Figure 4). On the other hand, in proliferating CAD 5 cells, there were 55.8% of cells in G0/G1, 25.6% in S and 18.1% in G2/M phase of the cell cycle.

3.6 | CAD 5 cells chronically infected with RML prions keep the infection after forming spheroids

CAD 5 RML cells formed spheroids similarly to their non-infected counterparts. Staining of fixed, paraffin-embedded slices of the infected spheroids with antibody

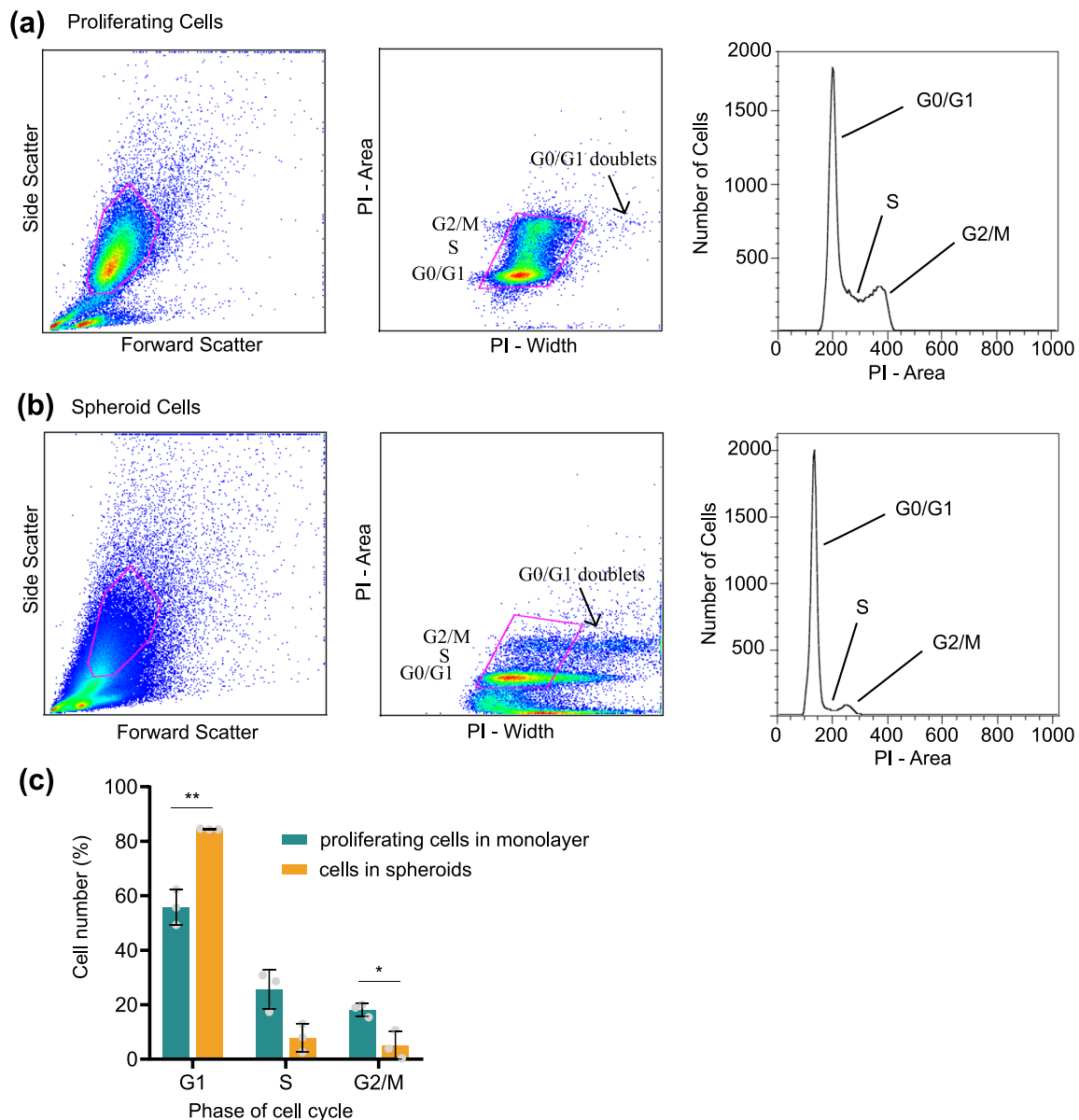


FIGURE 4 The majority of the spheroid cells are in the G1/G0 phase of the cell cycle. The scattergram shows the gating of the cell population harvested from the proliferating cells in monolayer (a) and from the spheroids (b). To exclude cell doublets, we plotted the area of the propidium iodide (PI) peak versus the width of the PI peak. The cell cycle was analysed using the Dean-Jett-Fox model. (c) Cell cycle analysis of proliferating cells in monolayer and spheroid cells. Mean \pm SD, $n = 3$, Welch two sample t test. * $p < .05$, ** $p < .01$.

6H4 demonstrated that practically all cells in the spheroids were positive for PrP^{TSE} (Figure 5a). The staining with antibody 12F10 provided a similar picture but stained the PrP^{TSE} with lower affinity (Figure 5b). The intensity of the signal varied among the cells. In some cells, aggregates of PrP^{TSE} were found (black arrows), and in others, there was only a tiny granular positivity of cytoplasm (red arrows). No signal was found in non-infected spheroid cells (data not shown). To confirm the cells' integrity, spheroids were also stained with haematoxylin and eosin (Figure 5c).

3.7 | CAD 5 cells chronically infected with RML prions in spheroids display a similar level of PrP^{TSE} as their proliferating counterparts in 2D monolayer

Western blot analysis of CAD 5 spheroids and proliferating CAD 5 cells, both chronically infected with RML, has demonstrated similar levels of PrP^{TSE} (Figure 6a,b). We also proved that the spheroids formed from non-infected CAD 5 cells can be infected de novo. The presence of PrP^{TSE} can be reliably detected starting 3 weeks after the exposition of spheroids to RML infectious inoculum, and the infection seems stable (Figure 6a, line 4).

3.8 | CAD 5 cells chronically infected with RML prions in 3D spheroid culture contain a higher level of prion converting activity than the proliferating cells in 2D monolayer

RT-QuIC assay analysis of serial dilutions of proliferating CAD 5 RML cells cultivated in monolayer has demonstrated the presence of prion converting activity up to 10^{-5} homogenate dilution (Figure 7a). In comparison, CAD 5 RML cells in 3-week-old spheroids provided the fluorescence signal up to 10^{-7} homogenate dilution (Figure 7b). The higher amount of prion converting activity in spheroids is documented by significant differences in the achieved maximal mean fluorescence (Figure 7c) and time to threshold (Figure 7d). Similar RT-QuIC results have been obtained also with 6-week-old CAD 5 RML spheroid culture (Figure S4A) and de-novo RML-infected spheroids (Figure S4B). Application of the Spearman-Kärber analysis on the collected data allowed calculation of the median prion seeding dose (SD_{50}) present in the studied cell homogenates. RML-infected spheroid cells have 1–2 orders of magnitude higher SD_{50} than the proliferating CAD 5 RML cells in the monolayer (Table 1).

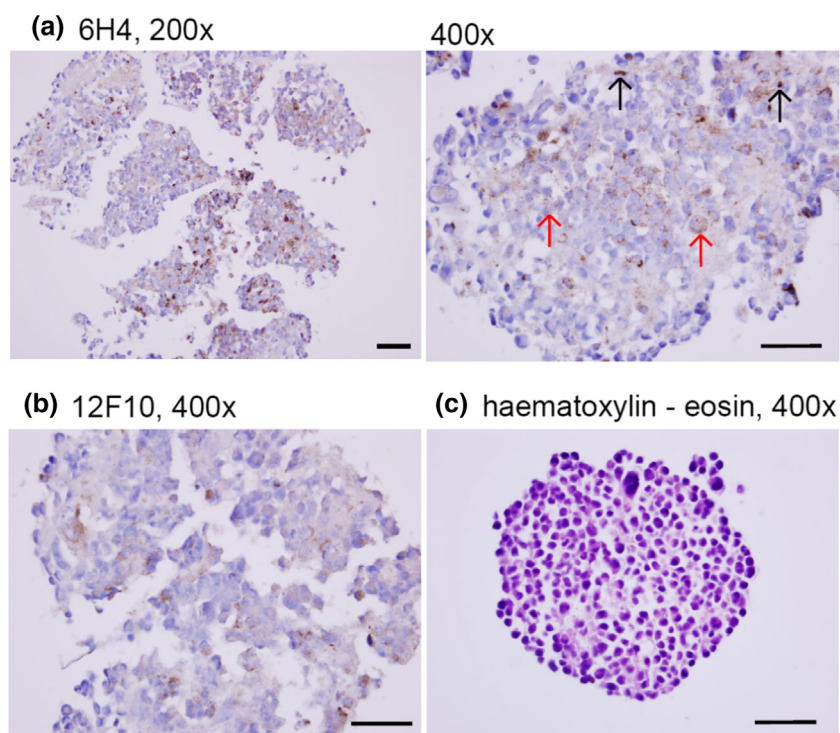


FIGURE 5 Spheroids formed from prion chronically infected CAD 5 cells keep the infection. Slices from fixed spheroids stained with 6H4 (a) and 12F10 (b) antibody recognizing PrP^{TSE} show the presence of Rocky Mountain Laboratory prion strain (RML) infection (brown). Black arrows: aggregates of PrP^{TSE}; red arrows: cytoplasmic granular positivity. (c) Spheroid stained with hematoxylin and eosin. Scale bar represents 100 μ m.

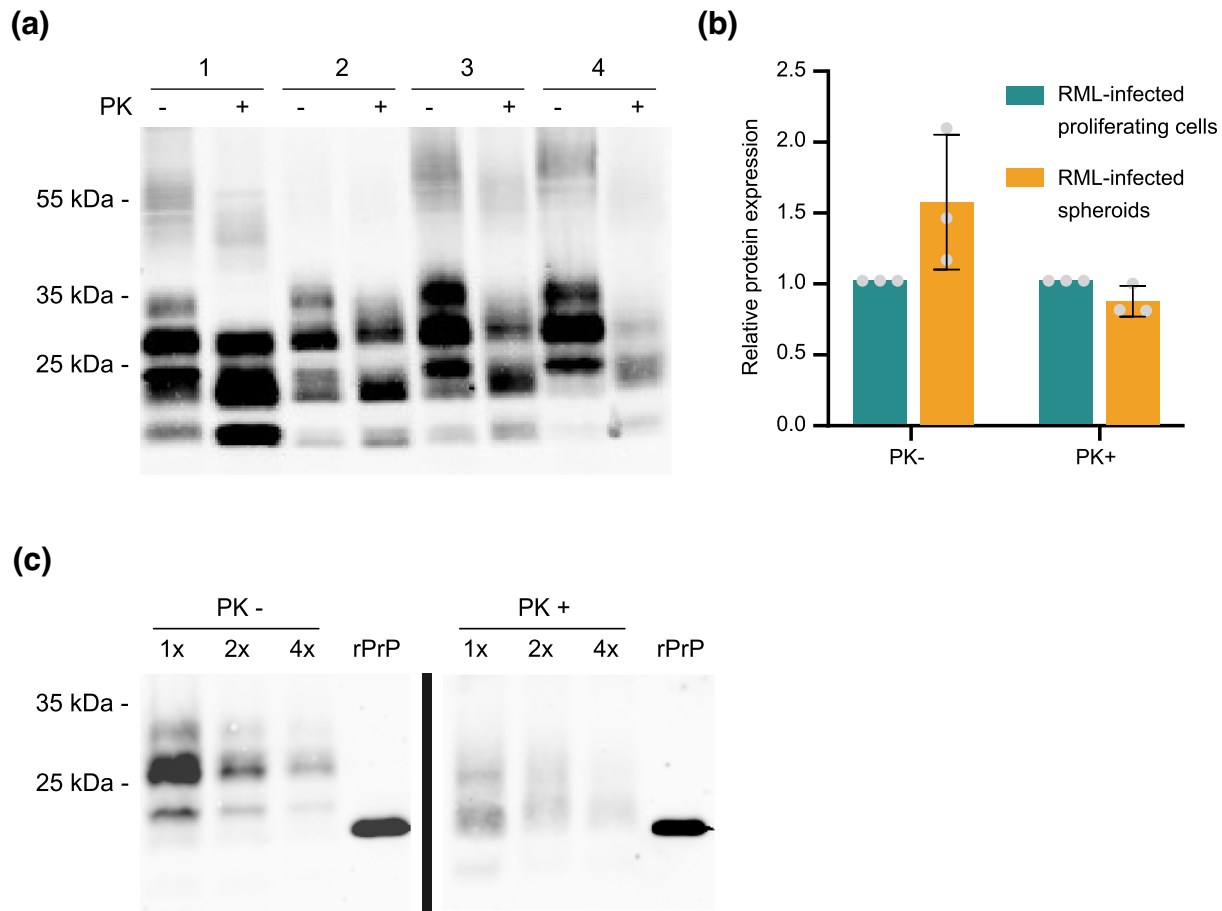


FIGURE 6 Western blot analysis confirms that PrP^{TSE} is present in spheroids derived from chronically infected CAD 5 cells as well as in de novo infected spheroids. (a) Rocky Mountain Laboratory prion strain (RML) brain homogenate used as a positive control (1). CAD 5 RML chronically infected cells cultured as proliferating monolayer (2) or spheroids (3). PrP^{TSE} was visualized after NaPTA precipitation and proteinase K (PK) treatment by immunostaining with the mixture of 6D11 and AH6 antibodies. (4) The presence of PrP^{TSE} in de novo infected spheroids 6 weeks after their exposure to infectious RML inoculum. (b) Densitometric analysis of total PrP (PK-) and PK resistant PrP^{TSE} (PK+) in the RLM chronically infected 2D proliferating cells and 3-week-old spheroids. Mean \pm SD, $n = 3$, t test. (c) Detection of PrP^{TSE} in the spheroids 3 weeks after their de novo infection with RML prions using western blot. The cell lysate was left untreated (PK-) or cleaved by proteinase K (PK+), subjected to NaPTA precipitation and serially diluted. Immunostaining was done as described above; recombinant prion protein (rPrP) was used as a control.

4 | DISCUSSION

Cell lines that divide rapidly may dilute out PrP^{TSE} inoculums as the cells replicate more quickly than PrP^{TSE} is formed (Ghaemmaghami et al., 2007). When using non-dividing cell culture, the accumulation of PrP^{TSE} may be much higher than in proliferating cells (Herbst et al., 2014). In addition, non-dividing cells better represent the in vivo situation of neuronal cells in the brain. In this study, we first attempted to gain more knowledge about the effect of prion infection on our 2D model of differentiated CAD 5 cells (Fremuntova et al., 2020). The differentiation process of the infected cells showed some delay, and the neurites grew slower compared with non-infected cells. This is in accord with studies where the

presence of PrP^{TSE} caused neurite retraction (Alleaume-Butaux et al., 2015; Fang et al., 2016), while PrP^C stimulated neurite outgrowth (Alleaume-Butaux et al., 2013; Amin et al., 2016; Loubet et al., 2012). It is not clear whether prion neurotoxicity is caused by the gain of function of toxic PrP^{TSE} or the loss of neuroprotective activity of PrP^C (Harris & True, 2006). The function of PrP^C in the differentiation process may be silenced by the dominance of PrP^{TSE}. It has been published that upregulation of PrP^C in human embryonic stem cells induced their differentiation, while PrP^C silencing caused the differentiation delay (Lee & Baskakov, 2013). Based on the loss-of-function hypothesis, the situation of prion infection may in some aspects resemble the situation of no PrP^C expression. For

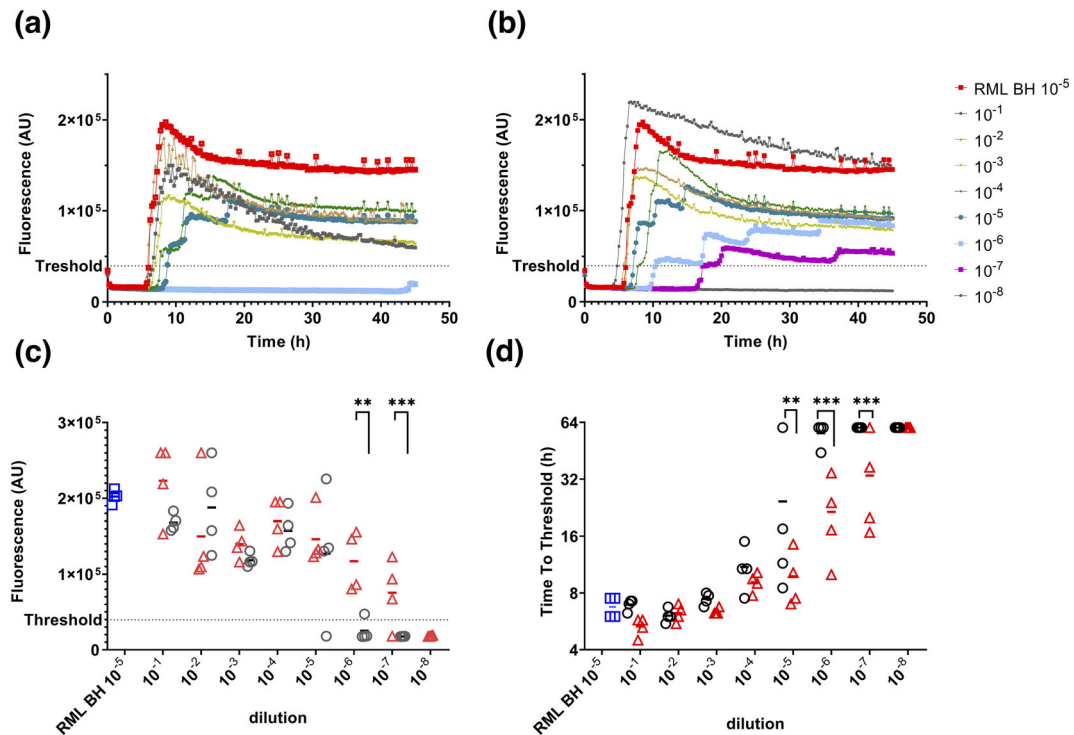


FIGURE 7 Real-time quaking-induced conversion (RT-QuIC) assay of Rocky Mountain Laboratory prion strain (RML)-infected CAD 5 cells grown in 2D monolayer and 3D spheroid culture. Kinetics of RT-QuIC reaction in serial dilution (10^{-1} – 10^{-8}) of the cells homogenate (1 g/L of protein) of (a) 2D RML chronically infected CAD 5 cells and (b) 3D RML chronically infected CAD 5 cells. (c) Comparison of max ThT fluorescence values of 2D (black circles) and 3D (red triangles) CAD 5 RML infected cell homogenates diluted 10^{-1} – 10^{-8} . (d) Comparison of time to threshold values between 2D and 3D CAD 5 RML infected cells. Individual values with arithmetic mean values are shown. A time of 60 h was assigned when the threshold was not reached. (** $p < .01$; *** $p < .001$). The threshold (39676 AU) was calculated as the arithmetic mean of maximal ThT fluorescence values of non-infected CAD 5 cells + 5 SD and is indicated by a dashed line. ThT fluorescence is expressed as arbitrary units AU. RML BH is brain homogenate from prion RML-infected mice.

TABLE 1 Comparison of median prion seeding dose (SD_{50}) of prion-infected CAD 5 cells cultured in monolayer (2D) or as spheroids (3D) estimated by RT-QuIC. CAD 5 cells chronically infected with RML prions (CAD 5 RML) were cultured in 2D or 3D conditions for 3 or 6 weeks. Eventually, a 1-week-old spheroid culture of CAD 5 cells was infected de novo by RML prions, and the spheroids were cultured for an additional 5 weeks. The representative mixed ($n = 2$) cell homogenates were prepared, and their serial dilutions were analysed by RT-QuIC in quadruplicates. The SD_{50} was calculated using the Spearman-Kärber method (Wilham et al., 2010).

Cells	Type of culture	Inoculum	Culture length (weeks)	$\log_{10} SD_{50}/2\text{-}\mu\text{l cell homogenate}$	$\log_{10} SD_{50}/\text{mg cell protein}$
CAD 5 RML	2D	n/a	3	5.25	7.95
CAD 5 RML	3D	n/a	3	7.25	9.95
CAD 5 RML	3D	n/a	6	6.50	9.20
CAD 5 RML	3D	RML	5	6.25	8.95

Abbreviations: RML, Rocky Mountain Laboratory prion strain; RT-QuIC, real-time quaking-induced conversion assay.

example, accumulation of PrP^{TSE} caused neurite retraction in cells expressing PrP^C, and at the same time, the PrP^{-/-} cells with no PrP^C expression showed shorter neurites compared PrP^C expressing cells (Fang et al., 2016; Kuwahara et al., 1999). In our previous study,

we showed that there was no difference in the dynamics of cell morphology change between CAD 5 PrP^{-/-} and CAD 5 PrP^{+/+} cells during the differentiation induced by serum withdrawal. However, CAD 5 PrP^{-/-} had slightly higher proliferating activity under normal culture

conditions (Fremuntova et al., 2020). Faster proliferation of PrP-knock-out neuronal cells has already been reported (Kim et al., 2005). This is in accord with our data demonstrating that the CAD 5 PrP^{-/-} cells continue proliferating longer after the serum withdrawal, and they return faster back to the proliferative status after dedifferentiation by serum inclusion. Interestingly, our experiments with differentiating RML-infected CAD 5 cells in 2D culture also suggested their somewhat slower response to induction of differentiation.

After verifying that prion infected CAD 5 cells are capable of differentiation, we have attempted to develop a 3D spheroid model by gradually changing cell culture conditions from the proliferative to the differentiating without serum. During the cultivation, the size of spheroids grew in time, reaching a plateau around the 14th day when most of them were visible to the eyes. This allows simple sampling, treatment and analysis of the individual spheroids in future studies. Spheroid differentiation may take longer than 5–7 days used in monolayer CAD 5 cell culture because the exchange of media and serum withdrawal is gradual. However, the interactions of the cells forming the spheroid may itself provide a differentiating signal. It was demonstrated in human neuroblastoma SH-SY5Y cells grown in 3D, which started differentiation without the necessity of its induction and had longer neurites than the cells differentiated in 2D (Seidel et al., 2012). The CAD 5 spheroids seem well formed without any inner cavity. Non-specific protein dye did not label the centre of the spheroids, suggesting that the packing of the cells limited the diffusion of the dye. The diminished ability of fluorescent dyes to penetrate deep inside the spheroids was noted before (Leary et al., 2018). This feature may make testing of any active compound (e.g. anti-prion drug) in our spheroid culture more stringent and closer to reality.

Differentiated cells stop dividing and are arrested in the G0 phase (Galderisi et al., 2003). The pool of undifferentiated cells remaining in the S and M-phase in CAD 5 spheroids was similar to what we described for the cells differentiated in a 2D monolayer (Fremuntova et al., 2020). The comparable pool of cells in the S and M-phase was also described in neurospheres generated from adipose-derived stem cells (Yang et al., 2015). In our hands, it was difficult to resuspend the spheroids to get a single-cell suspension, and many cells became fragmented. We faced the same problem when resuspending 2D differentiated CAD 5 cells, and we ascribed it to the fragility of long and thin neurites. Having the same problem now suggests a similar vulnerability of the cells in spheroids to mechanical stress as differentiated cells in 2D culture.

To analyse the differentiated status of the cells forming the spheroids, we examined the level of expression of various neuronal protein markers at the protein level. In 2D, we did not observe any difference in the expression of SNAP-25 and beta-III-tubulin after CAD 5 cells differentiation (Fremuntova et al., 2020), but in the spheroids, the expression of both markers was increased. This suggests the 3D environment may itself function as a differentiation stimulus. Similarly, in 3D neurosphere culture, the comparison of expression of neuronal markers as nestin, doublecortin and neurofilament-L showed increased neuronal differentiation over 2D cell culture (Collins & Haigh, 2017). In another model, after changing into a 3D cell culture, SHSY5Y cells expressed more beta-III-tubulin compared with the monolayer (Seidel et al., 2012). Expression of GFAP was significantly decreased in spheroid cells, indicating CAD 5 cells differentiate in the direction of neuronal cells because GFAP is a specific marker of astrocytes (Yang & Wang, 2015). GFAP was also detected in the ventral rostral hindbrain at E12 but not in neurospheres formed from this tissue (Osterberg & Roussa, 2009). The overall expression of PrP^C in the spheroid cells was significantly increased when compared with proliferating cells, as we described for 2D differentiated CAD 5 cells. However, PrP^C expression on the cell surface of spheroid cells was similar as in the proliferating cells. That differed from the 3-fold increase of the surface PrP^C expression in 2D differentiated cells. On the other hand, the decreased ratio of full-length and cleaved PrP^C on the plasma membrane of differentiated cells was similar in both 2D and 3D cultures and differed from the even ratio seen in the proliferating CAD 5 cells (Fremuntova et al., 2020). Our data suggest that while 2D and 3D differentiated cells share many similarities in the expression of differentiation markers, there are also some differences that may reflect a less artificial nature of the spheroid culture.

An important finding of our study was that the CAD 5 cells chronically infected with prions are capable of spheroid formation under the same conditions as the noninfected cells. The distribution of PrP^{TSE} through the CAD 5 RML spheroids was homogenous, and the cells kept the PrP^{TSE} quantity at the similar level as the RML infected proliferating cells in monolayer. We have expected to see more PrP^{TSE} accumulation in our 3D system, as the differentiated cells do not dilute their build-up by cell division. This suggests that some other factor is limiting the accumulation of PrP^{TSE} in the spheroids. The accumulation of PrP^{TSE} in the cell culture is affected by the interplay of PrP^{TSE} de novo formation, degradation, secretion, uptake and cell division (Ghaemmaghami et al., 2007). The importance and dynamics of these

processes in our 3D culture remain to be elucidated. In contrast to a similar level of PrP^{TSE} accumulation, the amount of prion-converting activity in the CAD 5 RML spheroids was markedly increased in comparison with the 2D infected culture. This finding suggests that PrP^{TSE} in the spheroid cells is more competent to initiate conformational change and aggregation of recombinant PrP substrate than PrP^{TSE} in the 2D culture. One possible but purely speculative explanation of this phenomenon is that the enhanced degradation of large PrP^{TSE} fibrils in the spheroids leads to an increased level of aggregation competent PrP^{TSE} oligomers and, at the same time, keeps the overall amount of PrP^{TSE} constant. Another important finding was that we were able to infect already formed CAD 5 spheroids with RML prions de novo, albeit the accumulation of detectable levels of PrP^{TSE} took noticeably longer than in the dividing CAD 5 cell culture. However, the level of prion converting activity in de novo infected spheroid culture detected by RT-QuIC was again higher compared with the infected 2D cultured cells. Previous studies of prion infection in 3D models suggested the presence of pathological changes observed in patient tissues, and we plan to investigate this interesting subject in our future studies.

5 | CONCLUSIONS

Our 3D culture model of differentiated CAD 5 cells provides an attractive model for further prion research because it is low cost, easy to produce and cultivable for weeks. In addition, as CAD 5 cells are known to propagate various prion strains, it can contribute to studies of prion strain differences. We anticipate the suitability of the CAD 5 spheroid model in testing anti-prion compounds and studies of factors affecting the dynamics of PrP^{TSE} accumulation. Furthermore, as the CAD cells have been previously used to study various aspects of neuronal pathophysiology, we foresee that our simple 3D spheroid model may also find utility outside the prion field.

AUTHOR CONTRIBUTIONS

Zuzana Fremuntova: Conceptualization; data curation; investigation; resources; writing - original draft. **Zdenka Backovska Hanusova:** Conceptualization; data curation; investigation; writing - original draft. **Jakub Soukup:** Conceptualization; data curation; investigation. **Tibor Mosko:** Formal analysis; investigation; visualization. **Radoslav Matej:** Data curation; investigation; writing - review and editing. **Karel Holada:** Conceptualization; funding acquisition; supervision; writing - review and editing.

ACKNOWLEDGEMENTS

The authors are grateful to Prof. Adriano Aguzzi, Prof. Dennis Burton, Prof. Vladka Curin Serbec, Prof. Charles Weissmann and the TSE Resource Centre for providing the material. The authors acknowledge the BioImaging Facility, Institute of Physiology, CAS supported by the MEYS CR (LM2015062 Czech-BioImaging) and ERDF (No.CZ.02.1.01/0.0/0.0/16_013/0001775) for their support with obtaining cell tomography data presented in this paper. The authors thank Ms Alena Steflava Lisakova for her excellent technical help. The study was supported by the Grant Agency of Charles University, project GAUK 530217, by the Ministry of Health of the Czech Republic, grant nr. NU23-04-00173 and by the project National Institute for Neurological Research (Programme EXCELES, ID Project No. LX22NPO5107) funded by the European Union – Next Generation EU.

CONFLICT OF INTEREST STATEMENT

The authors have declared no conflict of interest.

PEER REVIEW

The peer review history for this article is available at <https://www.webofscience.com/api/gateway/wos/peer-review/10.1111/ejn.16444>.

DATA AVAILABILITY STATEMENT

The datasets used and analysed in this study are freely available upon reasonable request to the corresponding author.

ORCID

Karel Holada  <https://orcid.org/0000-0002-3768-2629>

REFERENCES

- Ahn, M., Kalume, F., Pitstick, R., Oehler, A., Carlson, G., & DeArmond, S. J. (2016). Brain aggregates: An effective in vitro cell culture system modeling neurodegenerative diseases. *Journal of Neuro pathology and Experimental Neurology*, 75, 256–262. <https://doi.org/10.1093/jnen/nlv025>
- Alleaume-Butaux, A., Dakowski, C., Pietri, M., Mouillet-Richard, S., Launay, J. M., Kellermann, O., & Schneider, B. (2013). Cellular prion protein is required for neuritogenesis: Fine tuning of multiple signaling pathways involved in focal adhesions and actin cytoskeleton dynamics. *Cell Health and Cytoskeleton*, 5, 1–12.
- Alleaume-Butaux, A., Nicot, S., Pietri, M., Baudry, A., Dakowski, C., Tixador, P., Ardila-Osorio, H., Haeberlé, A. M., Bailly, Y., Peyrin, J. M., Launay, J. M., Kellermann, O., & Schneider, B. (2015). Double-edge sword of sustained ROCK activation in prion diseases through Neuritogenesis defects and prion accumulation. *PLoS Pathogens*, 11, e1005073. <https://doi.org/10.1371/journal.ppat.1005073>
- Amin, L., Nguyen, X. T., Rolle, I. G., D'Este, E., Giachin, G., Tran, T. H., Šerbec, V., Cojoc, D., & Legname, G. (2016).

- Characterization of prion protein function by focal neurite stimulation. *Journal of Cell Science*, 129, 3878–3891. <https://doi.org/10.1242/jcs.183137>
- Brandner, S., & Jaunmuktane, Z. (2017). Prion disease: Experimental models and reality. *Acta Neuropathologica*, 133, 197–222. <https://doi.org/10.1007/s00401-017-1670-5>
- Caughey, B., Standke, H. G., Artikis, E., Hoyt, F., & Kraus, A. (2022). Pathogenic prion structures at high resolution. *PLoS Pathogens*, 18, e1010594. <https://doi.org/10.1371/journal.ppat.1010594>
- Colby, D. W., & Prusiner, S. B. (2011). *Prions* (Vol. 3) (p. 3). Cold Spring Harb Perspect Biol. <https://doi.org/10.1101/cshperspect.a006833>
- Collins, S. J., & Haigh, C. L. (2017). Simplified murine 3D neuronal cultures for investigating neuronal activity and neurodegeneration. *Cell Biochemistry and Biophysics*, 75, 3–13. <https://doi.org/10.1007/s12013-016-0768-z>
- Didonna, A., Venturini, A. C., Hartman, K., Vranac, T., Curin Serbec, V., & Legname, G. (2015). Characterization of four new monoclonal antibodies against the distal N-terminal region of PrP(c). *PeerJ*, 3, e811. <https://doi.org/10.7717/peerj.811>
- Fang, C., Imberdis, T., Garza, M. C., Wille, H., & Harris, D. A. (2016). A neuronal culture system to detect prion synaptotoxicity. *PLoS Pathogens*, 12, e1005623. <https://doi.org/10.1371/journal.ppat.1005623>
- Fremuntova, Z., Mosko, T., Soukup, J., Kucerova, J., Kostelanska, M., Hanusova, Z. B., Filipova, M., Cervenakova, L., & Holada, K. (2020). Changes in cellular prion protein expression, processing and localisation during differentiation of the neuronal cell line CAD 5. *Biology of the Cell*, 112, 1–21. <https://doi.org/10.1111/boc.201900045>
- Galderisi, U., Jori, F. P., & Giordano, A. (2003). Cell cycle regulation and neural differentiation. *Oncogene*, 22, 5208–5219. <https://doi.org/10.1038/sj.onc.1206558>
- Ghaemmaghami, S., Phuan, P. W., Perkins, B., Ullman, J., May, B. C., Cohen, F. E., & Prusiner, S. B. (2007). Cell division modulates prion accumulation in cultured cells. *Proceedings of the National Academy of Sciences of the United States of America*, 104, 17971–17976. <https://doi.org/10.1073/pnas.0708372104>
- Giri, R. K., Young, R., Pitstick, R., DeArmond, S. J., Prusiner, S. B., & Carlson, G. A. (2006). Prion infection of mouse neurospheres. *Proceedings of the National Academy of Sciences of the United States of America*, 103, 3875–3880. <https://doi.org/10.1073/pnas.0510902103>
- Glier, H., & Holada, K. (2012). Blood storage affects the detection of cellular prion protein on peripheral blood leukocytes and circulating dendritic cells in part by promoting platelet satellitism. *Journal of Immunological Methods*, 380, 65–72. <https://doi.org/10.1016/j.jim.2012.04.002>
- González-González, M. A., Gómez-González, G. B., Becerra-González, M., & Martínez-Torres, A. (2017). Identification of novel cellular clusters define a specialized area in the cerebellar periventricular zone. *Scientific Reports*, 7, 40768. <https://doi.org/10.1038/srep40768>
- Grassmann, A., Wolf, H., Hofmann, J., Graham, J., & Vorberg, I. (2013). Cellular aspects of prion replication in vitro. *Viruses*, 5, 374–405. <https://doi.org/10.3390/v5010374>
- Harris, D. A., & True, H. L. (2006). New insights into prion structure and toxicity. *Neuron*, 50, 353–357. <https://doi.org/10.1016/j.neuron.2006.04.020>
- He, S., Park, Y. H., Yorio, T., & Krishnamoorthy, R. R. (2015). Endothelin-mediated changes in gene expression in isolated purified rat retinal ganglion cells. *Investigative Ophthalmology & Visual Science*, 56, 6144–6161. <https://doi.org/10.1167/iovs.15-16569>
- Herbst, A., Aiken, J. M., & McKenzie, D. (2014). Replication of prions in differentiated muscle cells. *Prion*, 8, 166–168. <https://doi.org/10.4161/pri.27890>
- Herva, M. E., Relano-Gines, A., Villa, A., & Torres, J. M. (2010). Prion infection of differentiated neurospheres. *Journal of Neuroscience Methods*, 188, 270–275. <https://doi.org/10.1016/j.jneumeth.2010.02.022>
- Hughes, D., & Halliday, M. (2017). What is our current understanding of PrP (Sc)-associated neurotoxicity and its molecular underpinnings? *Pathogens (Basel, Switzerland)*, 6, 6, 63. <https://doi.org/10.3390/pathogens6040063>
- Iwamaru, Y., Takenouchi, T., Imamura, M., Shimizu, Y., Miyazawa, K., Mohri, S., Yokoyama, T., & Kitani, H. (2013). Prion replication elicits cytopathic changes in differentiated neurosphere cultures. *Journal of Virology*, 87, 8745–8755. <https://doi.org/10.1128/JVI.00572-13>
- Jankovska, N., Rusina, R., Keller, J., Kukal, J., Bruzova, M., Parobkova, E., Olejar, T., & Matej, R. (2022). Biomarkers analysis and clinical manifestations in comorbid Creutzfeldt-Jakob disease: A retrospective study in 215 autopsy cases. *Biomedicine*, 10(3), 680. <https://doi.org/10.3390/biomedicines10030680>
- Janouskova, O., Rakusan, J., Karaskova, M., & Holada, K. (2012). Photodynamic inactivation of prions by disulfonated hydroxyaluminium phthalocyanine. *The Journal of General Virology*, 93, 2512–2517. <https://doi.org/10.1099/vir.0.044727-0>
- Kim, B. H., Kim, J. I., Choi, E. K., Carp, R. I., & Kim, Y. S. (2005). A neuronal cell line that does not express either prion or doppel proteins. *Neuroreport*, 16, 425–429. <https://doi.org/10.1097/00001756-200504040-00002>
- Kostelanska, M., & Holada, K. (2022). Prion strains differ in susceptibility to photodynamic oxidation. *Molecules (Basel, Switzerland)*, 27, 27. <https://doi.org/10.3390/molecules27030611>
- Kuwahara, C., Takeuchi, A. M., Nishimura, T., Haraguchi, K., Kubosaki, A., Matsumoto, Y., Saeki, K., Matsumoto, Y., Yokoyama, T., Itoharu, S., & Onodera, T. (1999). Prions prevent neuronal cell-line death. *Nature*, 400, 225–226. <https://doi.org/10.1038/22241>
- Lancaster, M. A., Renner, M., Martin, C. A., Wenzel, D., Bicknell, L. S., Hurles, M. E., Homfray, T., Penninger, J. M., Jackson, A. P., & Knoblich, J. A. (2013). Cerebral organoids model human brain development and microcephaly. *Nature*, 501, 373–379. <https://doi.org/10.1038/nature12517>
- Leary, E., Rhee, C., Wilks, B. T., & Morgan, J. R. (2018). Quantitative live-cell confocal imaging of 3D spheroids in a high-throughput format. *SLAS Technology*, 23, 231–242. <https://doi.org/10.1177/2472630318756058>
- Lee, W. J., Chen, L. C., Lin, J. H., Cheng, T. C., Kuo, C. C., Wu, C. H., Chang, H. W., Tu, S. H., & Ho, Y. S. (2019). Melatonin promotes neuroblastoma cell differentiation by activating

- hyaluronan synthase 3-induced mitophagy. *Cancer Medicine*, 8, 4821–4835. <https://doi.org/10.1002/cam4.2389>
- Lee, Y. J., & Baskakov, I. V. (2013). The cellular form of the prion protein is involved in controlling cell cycle dynamics, self-renewal, and the fate of human embryonic stem cell differentiation. *Journal of Neurochemistry*, 124, 310–322. <https://doi.org/10.1111/j.1471-4159.2012.07913.x>
- Levine, D. J., Stöhr, J., Falese, L. E., Ollesch, J., Wille, H., Prusiner, S. B., & Long, J. R. (2015). Mechanism of scrapie prion precipitation with phosphotungstate anions. *ACS Chemical Biology*, 10, 1269–1277. <https://doi.org/10.1021/cb5006239>
- Loubet, D., Dakowski, C., Pietri, M., Pradines, E., Bernard, S., Callebert, J., Ardila-Osorio, H., Mouillet-Richard, S., Launay, J. M., Kellermann, O., & Schneider, B. (2012). Neurotogenesis: The prion protein controls beta1 integrin signaling activity. *FASEB Journal: Official Publication of the Federation of American Societies for Experimental Biology*, 26, 678–690. <https://doi.org/10.1096/fj.11-185579>
- Mahal, S. P., Baker, C. A., Demczyk, C. A., Smith, E. W., Julius, C., & Weissmann, C. (2007). Prion strain discrimination in cell culture: The cell panel assay. *Proceedings of the National Academy of Sciences of the United States of America*, 104, 20908–20913. <https://doi.org/10.1073/pnas.0710054104>
- Martellucci, S., Santacroce, C., Santilli, F., Manganelli, V., Sorice, M., & Mattei, V. (2020). Prion protein in stem cells: A lipid raft component involved in the cellular differentiation process. *International Journal of Molecular Sciences*, 21, 4168. <https://doi.org/10.3390/ijms21114168>
- Matej, R., Olejar, T., Janouskova, O., & Holada, K. (2012). Deletion of protease-activated receptor 2 prolongs survival of scrapie-inoculated mice. *The Journal of General Virology*, 93, 2057–2061. <https://doi.org/10.1099/vir.0.043877-0>
- Moško, T., Galušková, S., Matěj, R., Brůžová, M., & Holada, K. (2021). Detection of prions in brain homogenates and CSF samples using a second-generation RT-QuIC assay: A useful tool for retrospective analysis of archived samples. *Pathogens*, 10(6), 750. <https://doi.org/10.3390/pathogens10060750>
- Osterberg, N., & Roussa, E. (2009). Characterization of primary neurospheres generated from mouse ventral rostral hindbrain. *Cell and Tissue Research*, 336, 11–20. <https://doi.org/10.1007/s00441-008-0743-0>
- Oz, S., Ivashko-Pachima, Y., & Gozes, I. (2012). The ADNP derived peptide, NAP modulates the tubulin pool: Implication for neurotrophic and neuroprotective activities. *PLoS ONE*, 7, e51458. <https://doi.org/10.1371/journal.pone.0051458>
- Panigaj, M., Glier, H., Wildova, M., & Holada, K. (2011). Expression of prion protein in mouse erythroid progenitors and differentiating murine erythroleukemia cells. *PLoS ONE*, 6, e24599. <https://doi.org/10.1371/journal.pone.0024599>
- Pozarowski, P., & Darzynkiewicz, Z. (2004). Analysis of cell cycle by flow cytometry. *Methods in Molecular Biology (Clifton, N.J.)*, 281, 301–311.
- Prusiner, S. B. (1998). Prions. *Proceedings of the National Academy of Sciences of the United States of America*, 95, 13363–13383. <https://doi.org/10.1073/pnas.95.23.13363>
- Qi, Y., Wang, J. K., McMillian, M., & Chikaraishi, D. M. (1997). Characterization of a CNS cell line, CAD, in which morphological differentiation is initiated by serum deprivation. *The Journal of Neuroscience: the Official Journal of the Society for Neuroscience*, 17, 1217–1225. <https://doi.org/10.1523/JNEUROSCI.17-04-01217.1997>
- Reynolds, B. A., & Weiss, S. (1992). Generation of neurons and astrocytes from isolated cells of the adult mammalian central nervous system. *Science (New York, N.Y.)*, 255, 1707–1710.
- Seidel, D., Krinke, D., Jahnke, H. G., Hirche, A., Kloss, D., Mack, T. G., Striggow, F., & Robitzki, A. (2012). Induced tauopathy in a novel 3D-culture model mediates neurodegenerative processes: A real-time study on biochips. *PLoS ONE*, 7, e49150. <https://doi.org/10.1371/journal.pone.0049150>
- Susaki, E. A., Tainaka, K., Perrin, D., Kishino, F., Tawara, T., Watanabe, T. M., Yokoyama, C., Onoe, H., Eguchi, M., Yamaguchi, S., Abe, T., Kiyonari, H., Shimizu, Y., Miyawaki, A., Yokota, H., & Ueda, H. R. (2014). Whole-brain imaging with single-cell resolution using chemical cocktails and computational analysis. *Cell*, 157, 726–739. <https://doi.org/10.1016/j.cell.2014.03.042>
- Uchiyama, K., Tomita, M., Yano, M., Chida, J., Hara, H., Das, N. R., Nykjaer, A., & Sakaguchi, S. (2017). Prions amplify through degradation of the VPS10P sorting receptor sortilin. *PLoS Pathogens*, 13, e1006470. <https://doi.org/10.1371/journal.ppat.1006470>
- Walters, R. O., & Haigh, C. L. (2023). Organoids for modeling prion diseases. *Cell and Tissue Research*, 392, 97–111. <https://doi.org/10.1007/s00441-022-03589-x>
- Watts, J. C., Bourkas, M. E. C., & Arshad, H. (2018). The function of the cellular prion protein in health and disease. *Acta Neuropathologica*, 135, 159–178. <https://doi.org/10.1007/s00401-017-1790-y>
- Wilham, J. M., Orrú, C. D., Bessen, R. A., Atarashi, R., Sano, K., Race, B., Meade-White, K. D., Taubner, L. M., Timmes, A., & Caughey, B. (2010). Rapid end-point quantitation of prion seeding activity with sensitivity comparable to bioassays. *PLoS Pathogens*, 6(12), e1001217. <https://doi.org/10.1371/journal.ppat.1001217>
- Williamson, R. A., Peretz, D., Pinilla, C., Ball, H., Bastidas, R. B., Rozenshteyn, R., Houghten, R. A., Prusiner, S. B., & Burton, D. R. (1998). Mapping the prion protein using recombinant antibodies. *Journal of Virology*, 72, 9413–9418. <https://doi.org/10.1128/JVI.72.11.9413-9418.1998>
- Yang, E., Liu, N., Tang, Y., Hu, Y., Zhang, P., Pan, C., Dong, S., Zhang, Y., & Tang, Z. (2015). Generation of neurospheres from human adipose-derived stem cells. *BioMed Research International*, 2015, 743714. <https://doi.org/10.1155/2015/743714>
- Yang, Z., & Wang, K. K. (2015). Glial fibrillary acidic protein: From intermediate filament assembly and gliosis to neurobiomarker. *Trends in Neurosciences*, 38, 364–374. <https://doi.org/10.1016/j.tins.2015.04.003>
- Ye, X., Feng, T., Tammineni, P., Chang, Q., Jeong, Y. Y., Margolis, D. J., Cai, H., Kusnecov, A., & Cai, Q. (2017). Regulation of synaptic amyloid-beta generation through BACE1 retrograde transport in a mouse model of Alzheimer's disease. *The Journal of Neuroscience: the Official Journal of the Society for Neuroscience*, 37, 2639–2655. <https://doi.org/10.1523/JNEUROSCI.2851-16.2017>
- Zhang, Q., Zhao, Y. F., Xi, J. Y., Yu, W. B., & Xiao, B. G. (2016). Rho kinase II interference by small hairpin RNA ameliorates

1methyl4phenyl1,2,3,6tetrahydropyridineinduced parkinsonism in mice. *Molecular Medicine Reports*, 14, 4947–4956. <https://doi.org/10.3892/mmr.2016.5889>

SUPPORTING INFORMATION

Additional supporting information can be found online in the Supporting Information section at the end of this article.

How to cite this article: Fremuntova, Z., Hanusova, Z. B., Soukup, J., Mosko, T., Matej, R., & Holada, K. (2024). Simple 3D spheroid cell culture model for studies of prion infection. *European Journal of Neuroscience*, 60(4), 4437–4452. <https://doi.org/10.1111/ejn.16444>